Weierstraß-Institut
für Angewandte Analysis und Stochastik

im Forschungsverbund Berlin e.V.

Preprint ISSN 0946 – 8633

Numerical investigation of the non-isothermal contact angle

Rolf Krahl[1], Eberhard Bänsch[2]

submitted: October 11, 2004

[1] Weierstraß-Institut
für Angewandte Analysis und Stochastik
Mohrenstraße 39
D–10117 Berlin
E-Mail: krahl@wias-berlin.de

[2] Friedrich-Alexander-Universität
Erlangen-Nürnberg
Lehrstuhl für Angewandte Mathematik III
Haberstraße 2
D–91058 Erlangen
E-Mail: baensch@mi.uni-erlangen.de

No. 972
Berlin 2004

2000 *Mathematics Subject Classification.* 76T10, 76D45, 80A20.

Key words and phrases. Two phase flow, free capillary surface, thermocapillarity, contact angle, Marangoni effect.

Edited by
Weierstraß-Institut für Angewandte Analysis und Stochastik (WIAS)
Mohrenstraße 39
10117 Berlin
Germany

Fax: + 49 30 2044975
E-Mail: preprint@wias-berlin.de
World Wide Web: http://www.wias-berlin.de/

Abstract

The influence of thermocapillary stress on the shape of the gas–liquid phase boundary is investigated numerically. We consider the case of a cold liquid meniscus at a heated solid wall in the absence of gravity. An "apparent contact angle" is defined geometrically and the deviation of this apparent contact angle from the prescribed static contact angle due to thermocapillary convection is studied.

1 Introduction

It is known from experiments that thermal effects have a considerable impact on the shape of a gas–liquid phase boundary and on the angle between this surface and a solid wall at the contact line. Gerstmann et al. investigated in [5] the reorientation of a gas–liquid phase boundary upon step reduction of gravity in the non-isothermal case. Our aim is similar, but we want to focus on the effect of Marangoni convection on the shape of the phase boundary. Therefore, we limit ourselves to the case where no external body forces act on the fluid.

2 Numerical setup

We mimic the experimental setup of Gerstmann et al. in our simulations, with the exception that the step reduction in gravity is skipped. More precisely, consider a circular cylinder with radius R, partly filled with liquid (see Fig. 1). The volume of the fluid is chosen to be $2\pi R^3$. That is, if the free surface of the fluid was completely flat, the filling height would be $2R$. We assume to have no gravity. In the isothermal case, the shape of the gas–liquid phase boundary is a sphere if the liquid is at rest. Now the cylinder wall is split in two parts: a cold one Γ_C, consisting of the bottom and the lower part of the wall up to a height of $1.8R$, and the upper part of the wall Γ_H, which is

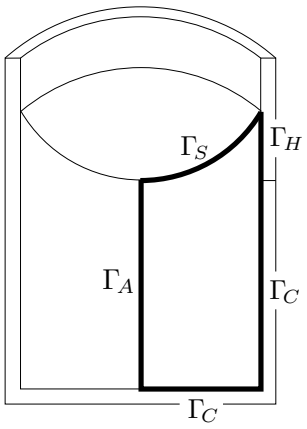

Figure 1: Computational domain

heated. The gas–liquid phase boundary Γ_S is assumed to be adiabatic. The liquid is cold initially.

The geometry of the setup and all boundary conditions are axial symmetric. We assume the solution to respect this symmetry, that is the azimuthal derivatives of all quantities involved, as well as the azimuthal component of the velocity are assumed to vanish.

2.1 Mathematical model

The flow field in the liquid region Ω is governed by the incompressible Navier–Stokes equations, which reads in an appropriate non-dimensional form as follows:

$$\begin{aligned} \partial_t \mathbf{u} + \mathbf{u}\cdot\nabla\mathbf{u} - \frac{1}{Re}\Delta\mathbf{u} + \nabla p &= \frac{Bo}{We}\mathbf{e}_g - \frac{Ra}{PrRe^2}\vartheta\mathbf{e}_g, \\ \nabla\cdot\mathbf{u} &= 0. \end{aligned} \tag{1}$$

The variables $\mathbf{u}$, p, and ϑ are the *dimensionless* velocity vector, the pressure, and the temperature respectively. $\mathbf{e}_g$ denotes the unit vector in the direction of the gravity.

No-slip boundary conditions are imposed at the cylinder wall:

$$\mathbf{u} = 0 \quad \text{on } \Gamma_C \cup \Gamma_H. \tag{2}$$

As an exception, slip boundary condition is imposed within a tiny region below the contact line in order to allow contact line to move up and down the cylinder wall.

At the phase boundary the stress is prescribed as a boundary condition for the flow:

$$\mathbf{T}\mathbf{n} = \frac{1}{We}(\nabla_S\cdot\mathbf{n})\mathbf{n} - \frac{Ma}{PrRe^2}\nabla_S\vartheta \quad \text{on } \Gamma_S. \tag{3}$$

$\mathbf{T} = -p\mathbf{I} + \frac{1}{Re}(\nabla\mathbf{u} + (\nabla\mathbf{u})^t)$ denotes the stress tensor, where $\mathbf{I}$ is the identity tensor. $\mathbf{n}$ denotes the outer normal to the free surface and ∇_S the gradient along the free surface. $\frac{1}{2}\nabla_S\cdot\mathbf{n}$ is the mean curvature of the free surface then.

The free surface moves with the normal component of the velocity:

$$\mathbf{u}\cdot\mathbf{n} = u_\Gamma. \tag{4}$$

A static contact angle γ_s is imposed as boundary condition for the free surface. More involved models for a dynamic contact angle could also be treated, but since the emphasis of this study is different, we keep the model for the contact angle as simple as possible.

For the heat transport, an advection-diffusion equation has to be solved:

$$\partial_t\vartheta + \mathbf{u}\cdot\nabla\vartheta - \frac{1}{PrRe}\Delta\vartheta = 0. \tag{5}$$

The phase boundary is assumed to be adiabatic:

$$\partial_{\mathbf{n}}\vartheta = 0 \quad \text{on } \Gamma_S. \tag{6}$$

At the walls, Dirichlet boundary conditions for the temperature are imposed. At Γ_C $\vartheta = 0$ is set. At the upper part of the cylinder wall Γ_H, the temperature starts with $\vartheta = 0$ in order to keep compatibility with the initial conditions. It is raised linearly with the time $\vartheta = \frac{1}{2}t$ in the time interval $0 < t < 2$ and kept at the level of $\vartheta = 1$ for $t \geq 2$.

As initial conditions, we start with the isothermal equilibrium configuration. The velocity and the temperature are set to zero, the free surface is set to a spherical shape.

2.2 Dimensionless numbers

The dimensionless parameters in (1–6) are defined as follows:

$Re = \frac{\rho U L}{\mu}$	Reynolds number,	$Bo = \frac{\rho g L^2}{\sigma}$	Bond number,
$We = \frac{\rho U^2 L}{\sigma}$	Weber number,	$Ra = \frac{g\rho^2 \beta_T \Theta L^3 c_p}{\lambda \mu}$	Rayleigh number,
$Pr = \frac{\mu c_p}{\lambda}$	Prandtl number,	$Re_M = \frac{Ma}{Pr} = \frac{\rho \sigma_T \Theta L}{\mu^2}$	thermocapillary Reynolds number,
$Ma = \frac{\sigma_T \Theta L \rho c_p}{\lambda \mu}$	Marangoni number.		

The material parameters ρ, μ, σ, c_p, λ, β_T, and σ_T are the density, the dynamic viscosity, the surface tension, the specific heat capacity, the heat conductivity, the thermal expansion coefficient, and $\sigma_T = -\frac{\partial \sigma}{\partial \vartheta}$ the dependency of the surface tension on temperature. The characteristic values U, L, Θ, and g are the characteristic velocity, the characteristic length, the characteristic temperature difference, and the characteristic acceleration.

In our case, we chose the characteristic length

$$L = R \tag{7}$$

to be the cylinder radius and the characteristic acceleration

$$g = 0 \, \frac{\mathrm{m}}{\mathrm{s}^2} \tag{8}$$

as we assume to have no gravity at all. The characteristic temperature difference Θ is the difference between the cold and the heated part of the wall. The driving force for the flow is the tangential stress at the phase boundary and thus, the tangential term in (3) should be in balance with the inertial term in (1). Therefore we chose the characteristic velocity

$$U = \sqrt{\frac{\sigma_T \Theta}{\rho L}}, \tag{9}$$

so that the factor $\frac{Ma}{PrRe^2}$ in the tangential stress term becomes unity. The characteristic time is given as $\frac{L}{U}$.

With this choice of characteristic values, we get

$$\begin{aligned} Re &= \sqrt{Re_M}, \\ We &= \frac{\sigma_T \Theta}{\sigma}, \\ Bo &= Ra = 0. \end{aligned} \tag{10}$$

Fixing for convenience $We = 0.2$ and $Pr = 15.0$, the free parameters of the simulations studied in this paper are Re_M and γ_s.

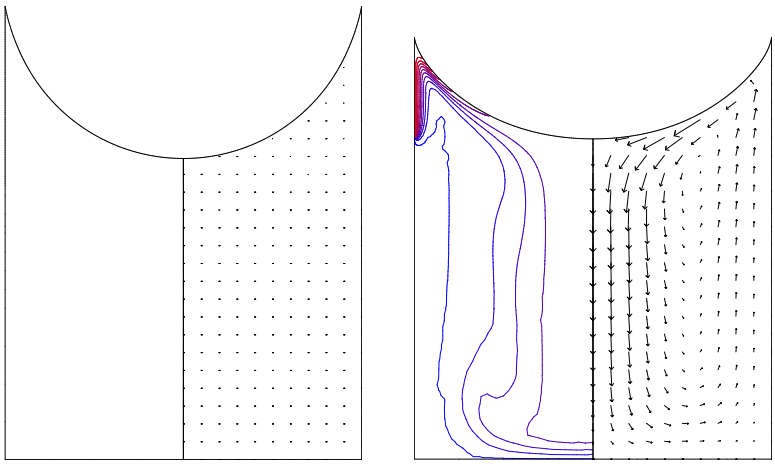

Figure 2: Shape of the free surface, isolines of temperature and velocity field in the isothermal initial configuration (left) and after the onset of thermocapillary convection (right).

3 Numerical methods

A finite element method is used to solve the numerical problem. The structure of the solver and the time discretization scheme is described in [1].

Key ingredient of the method for incorporating surface tension effects is the proper treatment of the free capillary boundary. To this end, a variational formulation for the curvature terms yields an accurate, dimensionally-independent and simple-to-implement approximation. The solver uses a stable time discretization, that is semi-implicit with respect to the treatment of the curvature terms. This firstly allows one to choose the time step independently of the mesh size—as opposed to common "explicit" treatments of the curvature terms—and secondly decouples the computation of the geometry and the flow field. This approach has proven to be both efficient and robust. For details see [2].

Applications of this method to some practical flow problems can be found for instance in [3, 4, 2].

4 Results

After the raise of the temperature at Γ_H, a temperature gradient induces a Marangoni stress at the phase boundary, exciting a flow in the liquid and a deformation of the free surface (Fig. 2).

As indicator for the deformation of the phase boundary, we study the vertical coordinate of the center of the free surface z_c and of the contact point of the surface with the cylinder wall z_w. Fig. 3 shows the typical behavior of the free surface in the simulations. The raise of temperature in Γ_H causes an initial deformation, characterized by a raise of z_c and a recede of z_w. After this deformation, the shape of the free surface changes only

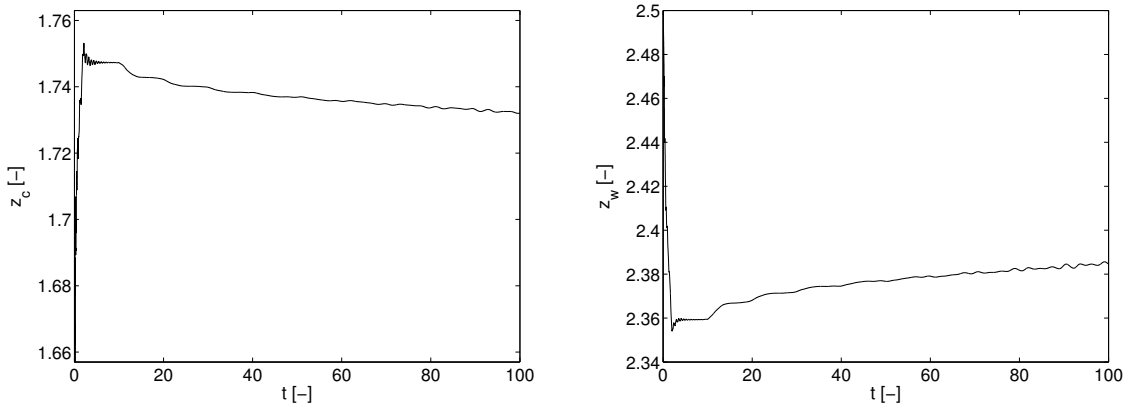

Figure 3: Vertical coordinate of the center point (left) and of the contact point (right) of the free surface vs. time. $Re_M = 2.5 \cdot 10^4$, $\gamma_s = 10°$.

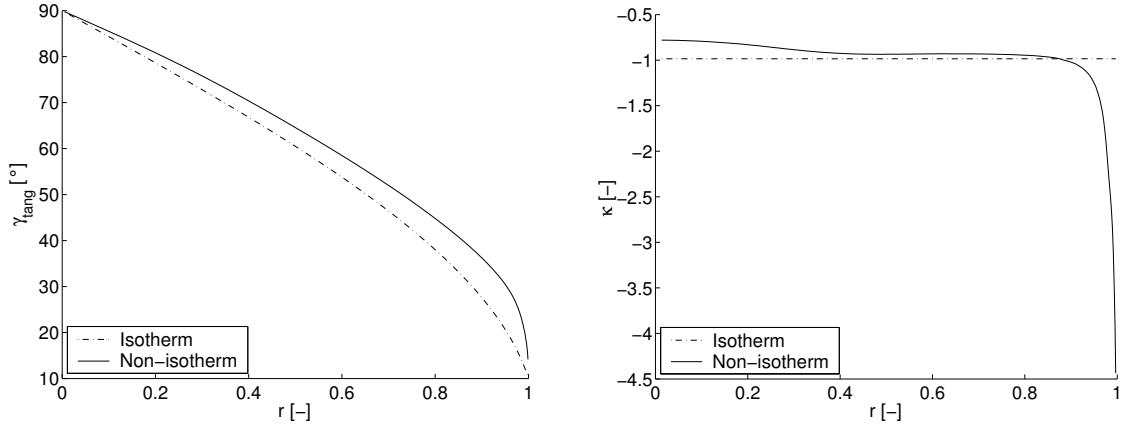

Figure 4: Angle of the tangent to the free surface and the vertical cylinder wall (left). Curvature of the free surface (right).

slowly in time, so that one may speak of a quasi-stationary state.

4.1 Shape of the non-isothermal free surface

The shape of the non-isothermal phase boundary has been evaluated at the instant $t = 23.0$. It is significantly flattened near the center compared to the isothermal initial configuration, resulting in a higher (flatter) angle between the tangent to the surface and the vertical cylinder wall (Fig. 4, left).

While the curvature of the free surface is constant in the isothermal configuration, it becomes much larger close to the cylinder wall in the non-isothermal case (Fig. 4, right).

One might assume that this strong variation in curvature within a small layer close to the wall is hardly visible to the eye. This could explain why the contact angle in the non-isothermal configuration *appears* to be higher than in the isothermal case, although the same contact angle was prescribed in both cases.

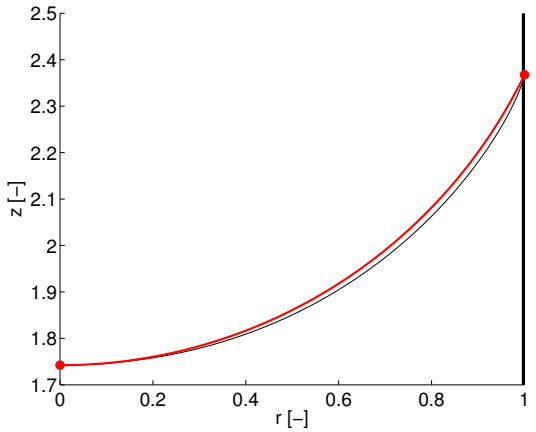

Figure 5: Approximation of the free surface by the circle connecting the center and the contact point.

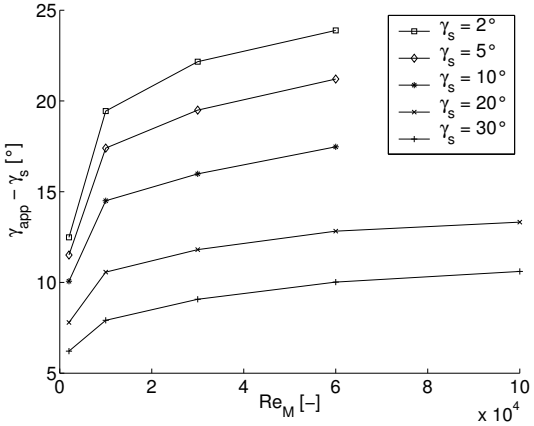

Figure 6: Deviation of the apparent contact angle from the prescribed static contact angle vs. Re_M for different static contact angles.

4.2 Apparent contact angle

In order to get a notion of a contact angle that corresponds to what may be observed in experiments, we define an "apparent contact angle" as follows: we approximate the free surface by the circle connecting the center and the contact point (Fig. 5). Now the *apparent contact angle* γ_{app} is defined to be the angle between the tangent of this circle and the vertical cylinder wall at the contact point.

Using this definition, the apparent contact angle is given by

$$\gamma_{app} = 90^\circ - 2\tan^{-1}(z_w - z_c). \tag{11}$$

Fig. 6 shows the deviation of γ_{app} from the prescribed static contact angle γ_s for different thermocapillary Reynolds numbers and for different values of γ_s. The trend of a larger apparent contact angle with increasing Re_M, as observed in the experiments, is confirmed by the numerical simulations.

But also the static contact angle γ_s turns out to play an important role: in case of a small γ_s, the convection role is more confined due to the narrower layer at the meniscus. In turn, the direction of the flow induced by the Marangoni stress that is pointing away from the wall forms a larger angle with the tangent of the surface, thus having a stronger effect on its shape.

For larger contact angles, the situation is opposite. The flow direction is more parallel to the surface and thus has a weaker influence on its shape.

5 Conclusions

As known from experiments, thermocapillarity has a considerable impact on the shape of a free capillary gas–liquid phase boundary. In the scenario of a cold liquid meniscus on a hot solid wall considered in this paper, we observe an enlarged apparent contact angle compared to the isothermal case. This effect has been confirmed and quantitatively studied in our numerical simulations.

We would like to emphasize that this effect does not depend on the specific model of a dynamic contact angle, since in our simulations a fixed static contact angle as boundary condition for the shape of the free surface has been used.

Acknowledgment

We like to thank the group of M. Dreyer from the Center of Applied Space Technology and Microgravity (ZARM) of Universität Bremen and in particular J. Gerstmann for the cooperation with this work and for many fruitful discussions.

This work has partly been supported by BMBF and DLR under grant 50 JR 0011 which is gratefully acknowledged.

A Nomenclature

A.1 Variables

$\mathbf{u}$	velocity vector	$[-]$
p	pressure	$[-]$
ϑ	temperature	$[-]$
t	time	$[-]$
u_Γ	normal velocity of the phase boundary	$[-]$

A.2 Material properties

c_p	specific heat capacity	$[\mathrm{J/(kg\,K)}]$
β_T	thermal expansion coefficient	$[\mathrm{1/K}]$
γ_s	static contact angle	$[^\circ]$
λ	heat conductivity	$[\mathrm{W/(K\,m)}]$
μ	dynamic viscosity	$[\mathrm{kg/(m\,s)}]$
ρ	density	$[\mathrm{kg/m^3}]$
σ	surface tension	$[\mathrm{N/m}]$
σ_T	dependency of the surface tension on temperature	$[\mathrm{N/(K\,m)}]$

A.3 Characteristic values

U	characteristic velocity	$[\mathrm{m/s}]$
L	characteristic length	$[\mathrm{m}]$
g	characteristic acceleration	$[\mathrm{m/s^2}]$
Θ	characteristic temperature difference	$[\mathrm{K}]$

A.4 Dimensionless numbers

Re	Reynolds number	$[-]$
We	Weber number	$[-]$
Pr	Prandtl number	$[-]$
Ma	Marangoni number	$[-]$
Bo	Bond number	$[-]$
Ra	Rayleigh number	$[-]$
Re_M	thermocapillary Reynolds number	$[-]$

A.5 Misc

R	radius of the cylinder	$[\mathrm{m}]$
Ω	liquid region	
Γ_C	lower wall part and bottom of the cylinder	
Γ_H	upper part of the cylinder wall	
Γ_S	gas–liquid phase boundary	
$\mathbf{n}$	outer normal to the phase boundary	$[-]$
$\mathbf{e}_g$	unit vector in the direction of the gravity	$[-]$
$\mathbf{I}$	identity tensor	$[-]$
$\mathbf{T}$	stress tensor	$[-]$
∇_S	gradient along the phase boundary	$[-]$
z_c	vertical coordinate of the center of the free surface	$[-]$
z_w	vertical coordinate of the contact point of the free surface	$[-]$
γ_{app}	apparent contact angle	$[^\circ]$

References

[1] E. Bänsch. Simulation of instationary, incompressible flows. *Acta Math. Univ. Comenianae*, 67(1), pp. 101–114, 1998.

[2] E. Bänsch. Finite element discretization of the Navier–Stokes equations with free capillary surface. *Numer. Math.*, 88(2), pp. 203–235, 2001.

[3] E. Bänsch, C. P. Berg, and A. Ohlhoff. Uniaxial, extensional flows in liquid bridges. *J. Fluid Mech.*, 2004. To appear.

[4] E. Bänsch and B. Höhn. Numerical simulation of a silicon floating zone with a free capillary surface. In F. Keil, W. Mackens, H. Voß, and J. Werther, eds., *Scientific computing in chemical engineering II*. Springer, 1999, volume 1, pp. 328–335.

[5] J. Gerstmann, M. Michaelis, and M. E. Dreyer. Capillary driven oscillations of a free liquid interface under non-isothermal conditions. *Proc. Appl. Math. Mech.*, 2004. To appear.